

## Electrochemical and Theoretical Studies of Novel Synthesized Benzimidazole Derivatives as Corrosion Inhibitors for Carbon Steel in 1 M HCl

Y. El Aoufir<sup>a,b</sup>, Y. El Bakri<sup>c</sup>, A. Chaouiki<sup>b,d</sup>, H. Lgaz<sup>b</sup>, H. Oudda<sup>b</sup>, R. Salghi<sup>d,\*</sup>, A. Guenbour<sup>a</sup> and E.M. Essassi<sup>c</sup>

<sup>a</sup> Laboratory of Nanotechnology, Materials & Environment, Faculty of Sciences, University Mohammed V, Rabat, Morocco

<sup>b</sup> Laboratory separation processes, Faculty of Science, University Ibn Tofail, P.O. Box 242, Kenitra, Morocco

<sup>c</sup> Laboratoire de chimie organique heterocyclique, URAC 21, Pôle de compétence pharmacochimie, Université Mohammed V, Faculté des sciences, Rabat, Maroc

<sup>d</sup> Laboratory of Environmental Engineering and Biotechnology, ENSA, University Ibn Zohr, P.O. Box 1136, 80000 Agadir, Morocco

Received March 6, 2018; accepted 18 September 2018

---

### Abstract

New corrosion inhibitors of benzimidazole derivatives, namely: 6-methoxy-2-(((4-methoxy-3,5-dimethylpyridin-2-yl)methyl)sulfinyl)-1-vinyl-1H-benzo[d]imidazole (EMSB), 6-Methoxy-2-(((4-methoxy-3,5-dimethylpyridin-2-yl)methyl)sulfinyl)-1-(prop-2-yn-1-yl)-1H benzimidazole (MSVB) and 6-methoxy-2-(((4-methoxy-3,5-dimethylpyridin-2-yl)methyl)sulfinyl)-1-(phenacyl)-1-H benzimidazole (MSBP), have been synthesized and their inhibiting action on the corrosion of carbon steel in acidic bath (1 M HCl) has been investigated by various corrosion monitoring techniques, such as weight loss measurement, potentiodynamic polarization, adsorption, electrochemical impedance spectroscopy (EIS) and basic computational calculations. The results of the investigation show that the inhibition efficiency of all the three inhibitors increases with increase in concentration of inhibitors and decreases with increase in temperature. The inhibitors, MSBP, MSVP, and EMSB show corrosion inhibition efficiency of 98, 97 and 93% respectively, at  $10^{-3}$  M and 303 K. EIS measurements showed an increase of the transfer resistance with the inhibitors concentration. Polarization studies showed that the studied inhibitors are mixed type in nature and the adsorption of benzimidazole is described by the Langmuir isotherm. In addition, density functional theory (DFT) calculations and molecular dynamics simulations (MDS) were undertaken to describe the electronic and adsorption properties of the synthesized inhibitors constituents, including the synergistic/dispersive interactive effects of the multiple adsorptions of the various active constituents in the inhibitor film on the iron surface. Also DFT and Molecular dynamic (MD) simulations were employed to correlate the experimental findings.

**Keywords:** inhibition; carbon steel; benzimidazole derivatives; acid solutions; DFT; molecular dynamic.

---

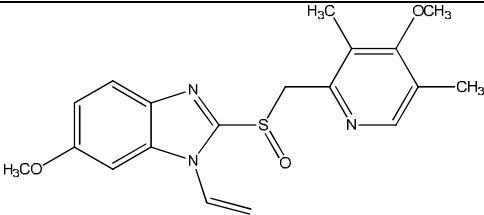
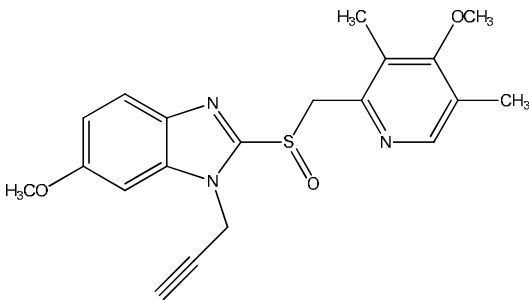
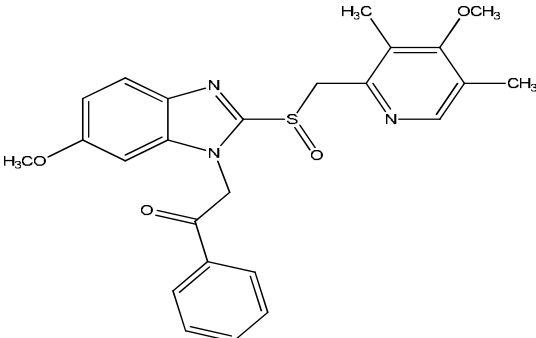
\* Corresponding author. E-mail address: r.salghi@uiz.ac.ma

## Introduction

Corrosion is an extremely widespread phenomenon, which tends to bring the metals towards the stable state, generally the oxide. It is a harmful (destructive, detrimental) phenomenon that is expensive, which causes the deterioration of a material by chemical or electrochemical action of its environment. For this, industries invested so much in preventing this scourge, because they depend immensely, for industrial operations, on metal and alloys which are prone to corrosion. The use of inhibitors is one of the most practical methods for protection against corrosion, especially in acidic solution. Many studies have been made on the corrosion and inhibition of steels in acidic media. The choice of the inhibitor is based on two considerations: first, economic consideration, and second, should contain the electron cloud on the aromatic ring or the electronegative atoms such as N, O, in the relatively long chain compounds. Generally the organic compounds containing hetero atoms like O, N, S, and P are found to work as very effective corrosion inhibitors. Recently, several researches have been carried out on the study of inhibition properties of benzimidazole and its derivatives for metallic corrosion[1–8]. We found that the efficiency depends on both the electronic and the chemical structure (molecular area and satiric distribution of the substituents) of the molecules, the influence of the latter being better expressed. Benzimidazole is a heterocyclic aromatic organic compound with a bicyclic structure consisting of the fusion of benzene and imidazole rings, and hydrogen atoms on the rings can be substituted by other groups or atoms. Some derivatives of benzimidazole have been demonstrated as excellent inhibitors for carbon steel in acidic media. Most efficient inhibitors in this class play important roles in retarding corrosion due to the presence of sites of adsorption for metal surface bonding; these sites are not limited to p-bonds and heteroatoms (P, S, N, O etc.) in which most of these compounds are endowed with. For benzimidazoles, the metal surface interaction takes place via the nitrogen atoms, and the strength of the inhibitor-metal bond is affected by the aromatic character of the compound and the presence of other substituent chemical groups connected with benzimidazole, which facilitates the adsorption of these compounds on the metallic surface [9-10]. The inhibition performance of benzimidazole has been investigated by both experimental methods and theoretical approaches. The present paper reports the inhibition action of three new benzimidazole derivatives, namely 6-methoxy-2-(((4-methoxy-3,5-dimethylpyridin-2-yl)methyl)sulfinyl)-1-vinyl-1H-benzo[d]imidazole (EMSB), 6-Methoxy-2-(((4-methoxy-3,5-dimethylpyridin-2-yl)methyl))sulfinyl)-1-(prop-2-yn-1-yl)-1H benzimidazole(MSVB) and 6-methoxy-2-(((4-methoxy-3,5-dimethylpyridin-2-yl)methyl)sulfinyl)-1-(phenacyl)-1-H-benzimidazole (MSBP). The molecular structures of the investigated organic compounds are shown in Table 1. The behavior of steel in 1.0 M HCl with and without inhibitor is studied using gravimetric, potentiodynamic and EIS measurements. The thermodynamic parameters for the adsorption process and activation parameters for steel dissolution reactions are determined and discussed. DFT together with Monte Carlo simulations (MC) are used to correlate the structural characteristics of the studied EMSB, MSVB and MSBP derivatives with their inhibition efficiencies,

and to ascertain their possible mode of adsorption on carbon steel in acidic solution.

**Table 1.** Abbreviation and chemical structures of the investigated organic compounds.

Abbreviation	Structural formula
EMSB (by1)	 <p><i>6-methoxy-2-(((4-methoxy-3,5-dimethylpyridin-2-yl)methyl)sulfinyl)-1-vinyl-1H-benzo[d]imidazole</i></p>
MSVB (by2)	 <p><i>6-Methoxy-2-(((4-methoxy-3,5-dimethylpyridin-2-yl)methyl)sulfinyl)-1-(prop-2-yn-1-yl)-1H-benzimidazole (MSVB)</i></p>
MSBP (by3)	 <p><i>6-methoxy-2-(((4-methoxy-3,5-dimethylpyridin-2-yl)methyl)sulfinyl)-1-(phenacyl)-1H-benzimidazole (MSBP)</i></p>

## Experimental section

### Synthesis of inhibitors

*6-Methoxy-2-(((4-methoxy-3,5-dimethylpyridin-2-yl)methyl)sulfinyl)-1-(prop-2-en-1-yl)-1H-benzimidazole (EMSB)*

To a solution of 6-methoxy-2-(((4-methoxy-3,5-dimethylpyridin-2-yl)sulfinyl)-1H-benzo[d]imidazole (1g, 2.89 mmol) in N,N-dimethylformamide (20 mL), potassium carbonate (0.4 g, 2.89 mmol), propargyl bromide (0.43 mL, 2.89 mmol) and a catalytic amount of tetra n-butylammonium bromide were added. The reaction mixture was stirred for 12 h. The solution was then concentrated to dryness under reduced pressure and the residue was extracted with dichloromethane. The precipitate formed by cooling was filtered and

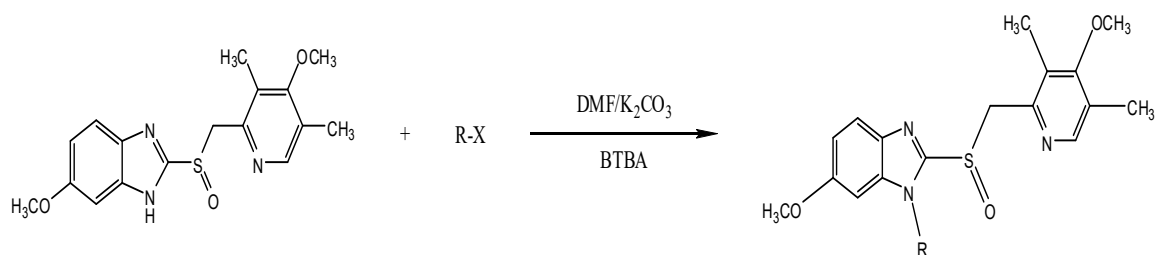
recrystallized from ethanol to give crystals with a yield of 65%. The compound was characterized by N.M.R. <sup>1</sup>H-NMR (DMSO-d<sub>6</sub>) (d ppm): 2.31(s,3H,CH<sub>3</sub>),2.81(s,1H,CH),3.83(s,3H;O-CH<sub>3</sub>),6.93(d,1H,CH<sub>aromatique</sub>), 7.48(d,1H,CH<sub>aromatique</sub>) 8.41(s,1H,CH-N) <sup>13</sup>C-NMR (DMSO-d<sub>6</sub>) (d ppm): 15.7(CH<sub>3</sub>), 55.8(O-CH<sub>3</sub>), 56.8(CH<sub>2</sub>), 58.3(HC triple liaison), 61.7(C triple liaison C), 100.8(C<sub>aromatique</sub>), 115(C-CH<sub>3</sub>), 116.2(C<sub>aromatique</sub>), 131.2(C-N), 158.5(C=N).

*6-Methoxy-2-(((4-methoxy-3,5-dimethylpyridin-2-yl)methyl)sulfinyl)-1-(prop-2-yn-1-yl)-1H-benzimidazole (MSVB)*

To a solution of 6-methoxy-2-(((4-methoxy-3,5-dimethylpyridin-2-yl)sulfinyl)-1H-benzo[d]imidazole(1 g, 2.89 mmol) in N,N-dimethylformamide (20 mL), potassium carbonate (0.4 g, 2.89 mmol), propargyl bromide (0.43 mL, 2.89 mmol) and a catalytic amount of tetra n-butylammonium bromide were added. The reaction mixture was stirred for 12 h. The solution was then concentrated to dryness under reduced pressure and the residue was extracted with dichloromethane. The precipitate formed by cooling was filtered and recrystallized from ethanol to give crystals with a yield of 65%.The compound was characterized by N.M.R. <sup>1</sup>H-NMR (DMSO-d<sub>6</sub>) (d ppm): 2.31(s,3H,CH<sub>3</sub>), 2.81(s,1H,CH), 3.83(s,3H;O-CH<sub>3</sub>), 6.93(d,1H,CH<sub>aromatique</sub>), 7.48(d,1H,CH<sub>aromatique</sub>) 8.41(s,1H,CH-N) <sup>13</sup>C-NMR (DMSO-d<sub>6</sub>) (d ppm):15.7(CH<sub>3</sub>), 55.8(O-CH<sub>3</sub>), 56.8(CH<sub>2</sub>), 58.3(HC triple liaison), 61.7(C triple liaison C), 100.8(C<sub>aromatique</sub>), 115(C-CH<sub>3</sub>), 116.2(C<sub>aromatique</sub>), 131.2(C-N), 158.5(C=N).

*6-methoxy-2-(((4-methoxy-3,5-dimethylpyridin-2-yl)methyl)sulfinyl)-1-(phenacyl)-1-H-benzimidazole (MSBP)*

To a solution of 6-methoxy-2-(((4-methoxy-3,5-dimethylpyridin-2-yl)sulfinyl)-1H-benzo[d]imidazole (1 g, 2.89 mmol) in N,N-dimethylformamide (20 mL), potassium carbonate (0.4 g, 2.89 mmol), phenacyl bromide ( 2.89 mmol) and a catalytic amount of tetra n-butylammonium bromide were added. The reaction mixture was stirred for 12 h. The solution was then concentrated to dryness under reduced pressure and the residue was extracted with dichloromethane. The precipitate formed by cooling was filtered and recrystallized from ethanol to give product with a yield of 60%.The compound was characterized by N.M.R. <sup>1</sup>H-NMR (DMSO-d<sub>6</sub>) (d ppm): 2.31(s,3H,CH<sub>3</sub>), 2.81(s,1H,CH), 3.83(s,3H;O-CH<sub>3</sub>), 6.22(s,2H,CH<sub>2</sub>), 6.93(d,1H,CH<sub>aromatique</sub>), 7.48(d,1H,CH<sub>aromatique</sub>) 8.41(s,1H,CH-N) <sup>13</sup>C-NMR (DMSO-d<sub>6</sub>) (d ppm): 15.7(CH<sub>3</sub>), 55.8(O-CH<sub>3</sub>), 56.8(CH<sub>2</sub>), 100.8(C<sub>aromatique</sub>), 115(C-CH<sub>3</sub>), 116.2(C<sub>aromatique</sub>), 131.2(C-N), 158.5(C=N), 190(C=O).



R = Allyl, Propargyl, Phenacyl

X = Br

General scheme

### Materials and sample preparation

Carbon steel specimens with the chemical composition (percentage): 0.36 wt.% C, 0.66 wt.% Mn, 0.27 wt.% Si, 0.02 wt.% S, 0.015 wt.% P, 0.21 wt.% Cr, 0.02 wt.% Mo, 0.22 wt.% Cu, 0.06 wt.% Al, and the rest iron, were used for all weight loss and electrochemical studies. Before exposing the specimens into the test solution, they were abraded and polished mechanically with 600, 800, 1000 and 1200 grade of emery paper, washed with double distilled water followed by acetone and finally dried in room temperature. The aggressive solutions, 1 M HCl, were prepared by dilution of analytical grade 37% HCl with distilled water. The concentration range of inhibitors employed was  $10^{-6}$  –  $10^{-3}$  M in 1 M HCl and the solution without inhibitor was prepared for comparison. All solutions were prepared using distilled water and were achieved in aerated medium under different temperatures (303, 313, 323 and 333 K).

### Weight loss tests

Identical coupons were immersed in 100 mL of aggressive solution with different concentrations of inhibitors at 303 K for 6 h. The specimens of the carbon steel used have a rectangular form (length = 2 cm, width = 2 cm, thickness = 0.08 cm). The coupons were weighed by an analytical balance with a precision of 0.1 mg before the tests. After the immersion, the coupons were taken out from the solution, and then they were washed with bristle brush under running water, degreased in acetone, rinsed with ethanol, dried by a hot air stream and re-weighed accurately. Three measurements were performed in each case and the mean value of the weight loss has been reported.

### Electrochemical methods

Potentiodynamic polarization and electrochemical impedance spectroscopy experiments were performed using a Volta laboratory (Tacussel- Radiometer PGZ 100) potentiostat and controlled by Tacussel corrosion analysis software model (Volta-master 4) at under static condition. The EIS data were fitted by Zview2 software. A conventional three-electrode system is used for potentiodynamic polarization and electrochemical impedance measurement. It consists of a carbon steel working electrode (WE) having the exposed area of 1 cm<sup>2</sup>, a platinum as counter electrode, and a saturated calomel electrode (SCE) as reference. Prior to each electrochemical test an immersion time of 30 min at open

circuit potential (OCP) was given to allow the system stabilization at corrosion potential. EIS tests in the absence and presence of the inhibitors were realized at free potential in the frequency range of 10 mHz to 100 kHz with the amplitude of the voltage perturbation 10 mV AC peak-to-peak at OCP. Nyquist plots were made from these experiments. Polarization resistance ( $R_p$ ), double layer capacitances ( $C_{dl}$ ) and other parameters were calculated by the fitting Nyquist plot. Polarization measurements were carried out in the range of the corrosion potential  $\pm 200$  mV/SCE. The scan rate was  $1 \text{ mV}\cdot\text{s}^{-1}$  as this value allowed the quasi-stationary state measurements. Electrochemical parameters such as corrosion current density ( $i_{corr}$ ), corrosion potential ( $E_{corr}$ ) and cathodic ( $\beta_c$ ) and anodic ( $\beta_a$ ) Tafel slopes were derived by extrapolation. Inhibition efficiencies were determined from corrosion currents calculated by the Tafel extrapolation method and fitting the linear part of the curve to the polarization equation.

### ***Quantum chemical studies***

Density Functional Theory (DFT) was performed to explore the relationship between inhibitor's molecular properties and inhibition efficiency. More accurate, DFT gives insights on the electronic and adsorption properties of some active constituents of inhibitors. DFT calculations for benzimidazole derivatives were carried out with the Lee–Yang–Parr nonlocal correlation functional (B3LYP) and 6-21G basis set implemented in Gaussian 09 program package [11]. In order to understand the reactivity of these compounds, several theoretical parameters such as the energies of the highest occupied and lowest unoccupied molecular orbitals ( $E_{HOMO}$  and  $E_{LUMO}$ , respectively), energy gap ( $\Delta E$ ), dipole moment ( $\mu$ ), global hardness ( $\eta$ ), softness ( $\sigma$ ) and fraction of electrons transferred from the inhibitor molecule to the metal surface ( $\Delta N$ ), were determined and discussed.

On the other hand, interaction energies between the studied benzimidazole derivatives and Fe(110) surface have been evaluated by Molecular Dynamics (MD) simulation technique using Materials Studio 7.0 (from Accelrys Inc.). The interaction of the inhibitor molecules with metallic surface was modelled based on the adsorption of a single inhibitor molecule on Fe(110) crystal surface. After constructing the initial geometry of the surface and inhibitor molecules, geometry optimization is done in order to get rid of the unfavorable structures and minimize the energy of the initial geometries. The structure of the inhibitor molecule was first optimized using the Condensed-phase Optimized Molecular Potentials for Atomistic Simulation Studies (COMPASS) force field. Fe crystal was cleaved into 110 plane to obtain a Fe(110) crystal plane. COMPASS force field was then used to optimize the surface to a minimum energy. The optimized Fe(110) was enlarged to a  $10 \times 10$  supercell and a vacuum slab of zero thickness was built above the plane. A supercell with a size of  $a = b = 24.82 \text{ \AA}$ ,  $c = 25.14 \text{ \AA}$ , contains 500  $\text{H}_2\text{O}$ , 9  $\text{Cl}^-$ , 9  $\text{H}_3\text{O}^+$  and a molecule of tested benzimidazole derivatives was created. The MD simulation is performed under canonical ensemble (NVT) at a temperature of 298 K using a time step of 1.0 fs and simulation time of 100 ps. The adsorption strengths between the inhibitor species and Fe(110) can be evaluated by calculating the interaction energies using the following equations [12]:

$$E_{\text{interaction}} = E_{\text{total}} - (E_{\text{surface+solution}} + E_{\text{inhibitor}}) \quad (1)$$

$$E_{\text{Binding}} = -E_{\text{interaction}} \quad (2)$$

where  $E_{\text{total}}$  is the total energy of the entire system,  $E_{\text{surface+solution}}$  is the energy of iron surface and solution without the inhibitor, and  $E_{\text{inhibitor}}$  represents the total energy of the inhibitor.

## Results and discussion

### *Effect of inhibitor concentration*

#### *Weight loss study*

The corrosion of carbon steel in 1 M HCl solution containing various concentrations of the inhibitors EMSB, MSVB and MSBP, after 6 h of immersion at 303 K was evaluated by the weight loss technique. The corrosion rate ( $W$ ), inhibition efficiency  $\eta_{\text{WL}}(\%)$  and surface coverage obtained by the weight loss measurements for carbon steel are listed in Table 2. The following equations were used to calculate the inhibition efficiency and the surface coverage ( $\theta$ ):

$$\eta_{\text{WL}}(\%) = \left[ \frac{W^\circ - W}{W^\circ} \right] \times 100 \quad (3)$$

$$\theta = \left[ \frac{W^\circ - W}{W^\circ} \right] \quad (4)$$

where  $W$  and  $W^\circ$  are the corrosion rates of carbon steel with and without inhibitors, respectively, and  $\theta$  is the degree of surface coverage of the inhibitors. The corrosion rate was calculated from the weight loss. Fig. 1a illustrates the influence of the increasing concentrations of the tested inhibitors on the corrosion rate of CS in 1M HCl acid solution. It is obvious that the corrosion rate decreases with increasing inhibitor concentration, which suggests the retardation of CS corrosion in the presence of benzimidazole derivatives with respect to the plain acid (1 M HCl).

The variation in the inhibition efficiency of benzimidazole derivatives with their concentrations is shown in Fig. 1b. It seems from this figure that the inhibition efficiency,  $\eta_{\text{WL}}(\%)$ , of the studied inhibitors increases with increasing their concentration, reaching a maximum at  $10^{-3}$  M of all the tested molecules. It is further evident that all the three inhibitors show appreciably high  $\eta_{\text{WL}}(\%)$  even at a concentration as low as  $10^{-6}$  M. The inhibitors efficiencies of EMSB, MSVB and MSBP were found to be 90, 93 and 94%, respectively, at  $10^{-3}$  M, and 68, 79 and 85%, respectively, at  $10^{-6}$  M and 303 K (Table 2). The increase in  $\eta_{\text{WL}}(\%)$  with increasing the concentration of inhibitors was due to increase in the surface coverage, which results in enhanced retardation of metal dissolution in the

aggressive media [13]. MSBP with three N, one S and four O-atoms in its molecules showed better inhibition performance than EMSB and MSVB with three N, one S and three O-atoms each. This further supports previous reports that the presence of heteroatoms in an organic molecule facilitates adsorption onto metal surface and enhances corrosion inhibition [14–16].

**Table 2.** Corrosion rate and inhibition efficiency of various concentrations of benzimidazole derivates for corrosion of carbon steel in 1 M HCl obtained by weight loss measurements at 303 K.

Inhibitors	Concentration (M)	$W$ ( $\text{mg}/\text{cm}^2 \times \text{h}$ )	$\eta_{WL}$ (%)	$\theta$
Blank	1	1.135	-	-
EMSB	$1 \times 10^{-6}$	0.363	68	0.68
	$1 \times 10^{-5}$	0.249	78	0.78
	$1 \times 10^{-4}$	0.181	84	0.84
	$1 \times 10^{-3}$	0.113	90	0.90
MSVB	$1 \times 10^{-6}$	0.238	79	0.79
	$1 \times 10^{-5}$	0.192	83	0.83
	$1 \times 10^{-4}$	0.102	91	0.91
	$1 \times 10^{-3}$	0.079	93	0.93
MSBP	$1 \times 10^{-6}$	0.170	85	0.85
	$1 \times 10^{-5}$	0.124	89	0.89
	$1 \times 10^{-4}$	0.091	92	0.92
	$1 \times 10^{-3}$	0.068	94	0.94

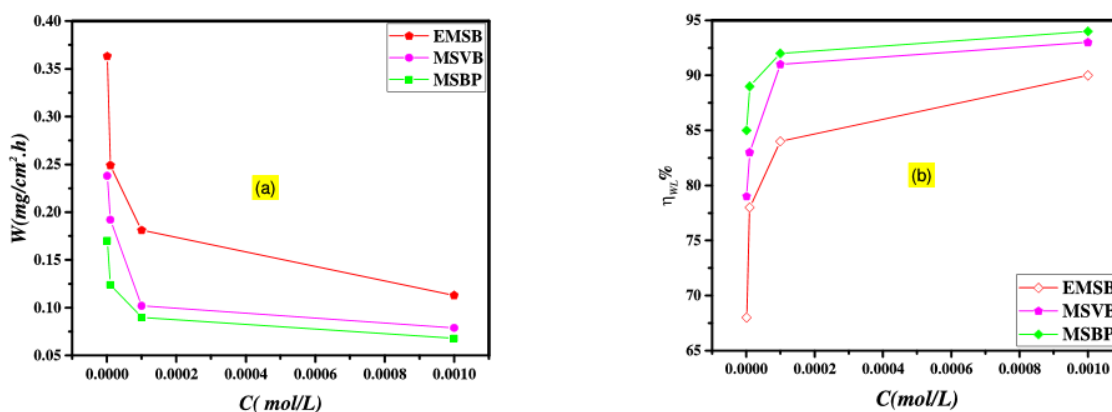


**Figure 1.** Variation of the concentration of benzimidazoles' derivates with (a)  $W$  and (b)  $\eta_{WL}$  (%) of carbon steel in 1 M HCl solution.



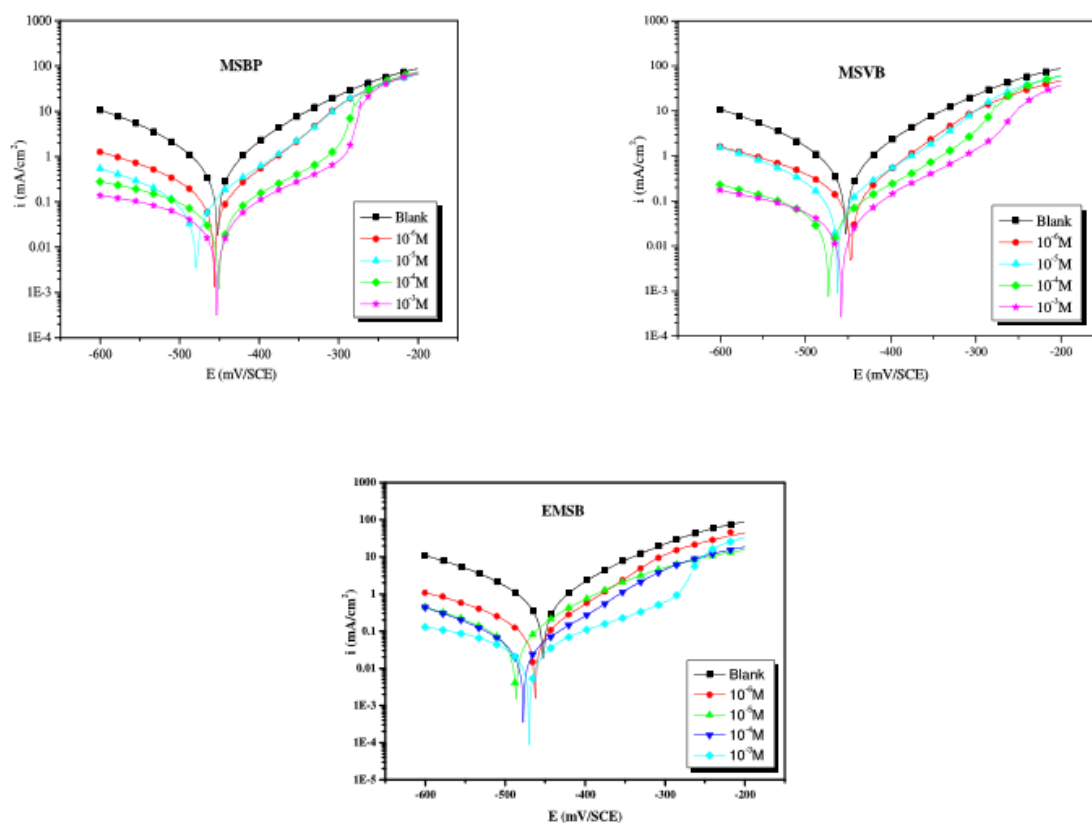


**Figure 2.** Potentiodynamic polarization curves for carbon steel in 1 M HCl without and with different concentrations of EMSB, MSVB and MSBP.

### Potentiodynamic polarization curves

Polarization is an opposite measurement to identify the effect of inhibitor on both anodic and cathodic reactions. Potentiodynamic polarization curves of CS in 1 M HCl without and with different concentrations of benzimidazole derivates at 303 K are given in Fig. 2. The electrochemical parameters were obtained by extrapolating the anodic and cathodic Tafel regions of the curves to the point of intersection with the  $E_{\text{corr}}$ . The corrosion inhibition efficiency  $\eta_{\text{PDP}}(\%)$  was calculated using the relation:

$$\eta_{\text{PDP}}(\%) = \left[ 1 - \frac{i_{\text{corr}}}{i_{\text{corr}}^{\circ}} \right] \times 100 \quad (5)$$

where  $i_{\text{corr}}$  and  $i_{\text{corr}}^{\circ}$  are the corrosion current density in inhibited and uninhibited acid, respectively. Values of  $i_{\text{corr}}$ , corrosion potential ( $E_{\text{corr}}$ ),  $\eta_{\text{PDP}}(\%)$ , cathodic and anodic Tafel line as function of benzimidazole derivatives concentrations, are given in Table 3.

**Table 3.** Electrochemical parameters for carbon steel in 1 M HCl at various concentrations of EMSB, MSVB and MSBP at 303 K.

Inhibitors	Concentration (M)	$-E_{\text{corr}}$ (mV/SCE)	$i_{\text{corr}}$ ( $\mu\text{A cm}^{-2}$ )	$\beta_a$ (mV dec $^{-1}$ )	$-\beta_c$ (mV dec $^{-1}$ )	$\eta_{\text{PDP}}$ (%)	$\theta$
HCl	1.0	452	507	100	122	-	-
	$1 \times 10^{-6}$	465.1	126.5	84.5	148.6	75	0.75
EMSB	$1 \times 10^{-5}$	489.6	101.0	103.5	176.7	80	0.80
	$1 \times 10^{-4}$	480.1	52.1	93.3	139.3	89	0.89
	$1 \times 10^{-3}$	472.4	40.2	159	161	92	0.29
MSVB	$1 \times 10^{-6}$	446	96	71	100	81	0.81
	$1 \times 10^{-5}$	462	71	84	87	86	0.86
	$1 \times 10^{-4}$	473	35	92	133	93	0.93
	$1 \times 10^{-3}$	457	25	81	135	95	0.95
MSBP	$1 \times 10^{-6}$	455	51	62	74	90	0.90
	$1 \times 10^{-5}$	479	36	78	89	93	0.93
	$1 \times 10^{-4}$	451	20	61	75	96	0.96
	$1 \times 10^{-3}$	453	15	65	97	97	0.97

Polarization curves in Fig. 2 show that the addition of these organic compounds (benzimidazoles derivatives) to the corrosive medium (1M HCl) leads to a decrease in the densities of cathodic and anodic currents. This effect is all the more marked when the concentration of added compounds increases. These results suggest that benzimidazoles reduce anodic dissolution and delay the reduction of  $\text{H}^+$  protons. The polarization curves show a slight shift of the corrosion potential to more negative values. An inhibitor may be classified as of a cathodic or anodic type if the displacement in corrosion potential is greater than 85 mV with respect to the corrosion potential of the control solution [17]. In our study, the maximum displacement is less than 85 mV/  $E_{\text{corr}}$ , which indicates that the organic compounds act as mixed-type inhibitors.

In the cathodic domain, the addition of the inhibitors in corrosive medium results in a significant decrease in the cathodic partial current as well as a slight modification of the cathode Tafel slopes. These branches have a wide range of linearity, which proves that Tafel's law is well verified in this domain. These observations show that the reduction reaction of  $\text{H}^+$  protons on the surface of carbon steel is not modified by the addition of inhibitors and that it is carried out according to a pure activation mechanism. The inhibitor appears to be adsorbed first on the surface of the metal before acting by simple blocking of the active sites [18]. The results of table 3 show that the values of  $i_{\text{corr}}$  determined by extrapolation of the cathodic lines of the polarization curves decrease as the concentration of inhibitors increases, and the values of  $\eta_{\text{PDP}}(\%)$  increase with

concentration and reached a maximum of 92 %, 95%, and 97%, respectively, at  $10^{-3}$  M for EMSB, MSVB, and MSBP. Observed trend manifests that the phenacyl substituted MSBP derivative has better blocking ability than those of the alkyl chains substituted derivatives. The potentiodynamic data confirm the conclusions of the gravimetric tests, giving some additional information about the type of inhibition.

### ***Electrochemical Impedance Spectroscopy (EIS)***

Electrochemical impedance spectroscopy (EIS) allows the study of the resistive and capacitive behavior at the interface and makes it possible to evaluate the performance of the compounds tested as corrosion inhibitors of metals. Nyquist plots were shown in Fig. 3 for carbon steel in 1M HCl solution without and with different concentration of EMSB, MSVB and MSBP. Fig. 3 shows that the impedance patterns have the shape of a depressed semicircle. It is clear from this fig. that the impedance response of CS (diameter of the semicircle) has changed considerably after the addition of inhibitors in the corrosive solution. Though the curves are in the depressed form, the diameter of the semi circle increased at each higher concentration level, related to decrease in active sites. This suggests that the metal surface was protected from acidic environment and maximum protection was attained at optimum concentration which afforded highest inhibition efficiency. It should be noted that the modification of EMSB, MSVB and MSBP concentrations did not alter the shape of the impedance behavior, suggesting a similar mechanism for the inhibition of corrosion of carbon steel by these inhibitors. High resistance to charge transfer is associated with a slow corrosion system.

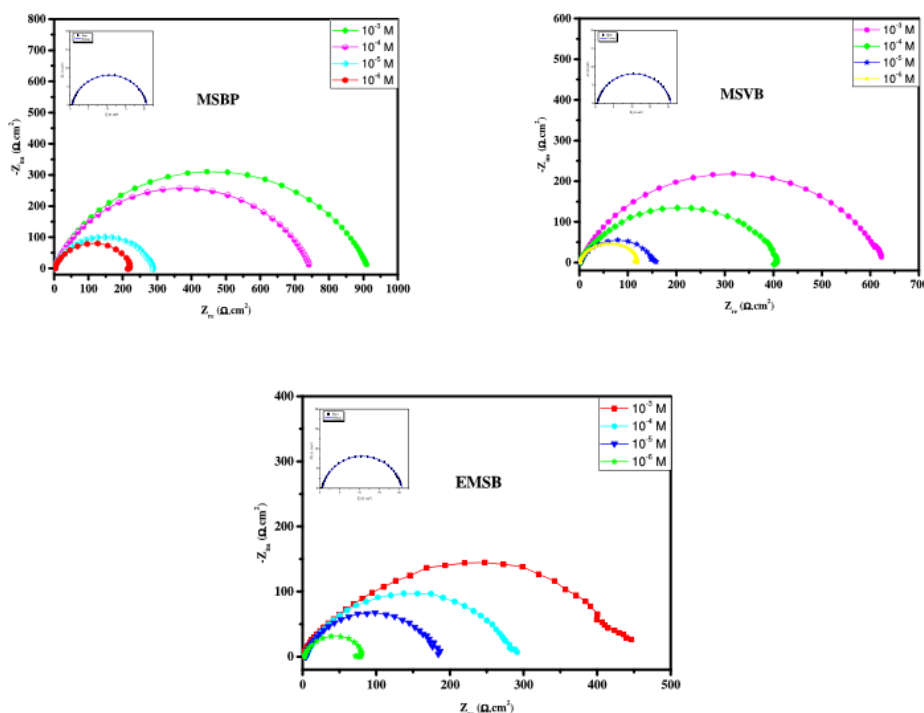


**Figure 3.** Nyquist plots for carbon steel in 1.0 M HCl solution in the absence and presence of various concentrations of benzimidazole derivatives.

The best fit equivalent circuit applied for fitting of the impedance data was presented in Fig. 4. The EIS parameters were determined and listed in Table 4. This circuit comprises parallel combination of the charge transfer resistance ( $R_{ct}$ ) and the constant phase element (CPE), both in series with the solution resistance ( $R_s$ ). This type of electrochemical equivalent circuit was reported previously to model the iron/acid interface [19]. Considering that the impedance of a double layer does not behave as an ideal capacitor in the presence of a dispersion effect, a constant phase element CPE is used as a substitute for the capacitor in Fig. 4 to more accurately match the impedance behavior of the electrical double layer. Constant phase elements have largely been used to account for deviations caused by surface roughness. This circuit gives an exact fit to all experimental impedance data for our inhibitors.

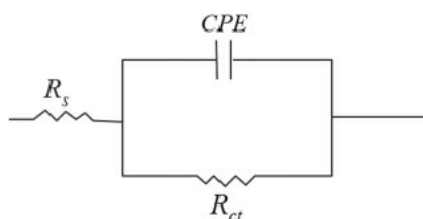


**Figure 4.** Equivalent circuit used to model impedance data.

**Table 4.** Electrochemical impedance parameters for carbon steel in 1.0 M HCl solution without and with different concentrations of benzimidazole derivatives at 303 K.

Medium	Concentration (M)	$R_s$ ( $\Omega \text{ cm}^2$ )	$R_{ct}$ ( $\Omega \text{ cm}^2$ )	$Q \times 10^{-4}$ ( $\Omega^{-1} \text{ cm}^{-2} \text{ s}^n$ )	n	$C_{dl}$ ( $\mu\text{F cm}^{-2}$ )	$\eta_{R_{ct}}$ (%)
Blank	1.0	0.568	20.24	2.420	0.860	112.04	-
EMSB	$1 \times 10^{-6}$	0.961	67.2	1.430	0.81	48.09	69
	$1 \times 10^{-5}$	1.826	126.0	0.762	0.85	33.56	83
	$1 \times 10^{-4}$	1.840	202.0	0.930	0.75	26.72	89
	$1 \times 10^{-3}$	0.760	335.0	0.567	0.81	22.37	93
MSVB	$1 \times 10^{-6}$	1.247	119.2	1.020	0.82	41.09	83
	$1 \times 10^{-5}$	1.407	150.7	0.942	0.80	32.97	87
	$1 \times 10^{-4}$	1.062	406.4	0.810	0.74	25.39	95
	$1 \times 10^{-3}$	1.067	621.2	0.563	0.78	21.99	97
MSBP	$1 \times 10^{-6}$	1.309	221.1	0.830	0.80	31.32	91
	$1 \times 10^{-5}$	1.215	283.5	0.780	0.79	29.54	93
	$1 \times 10^{-4}$	1.012	738.7	0.501	0.78	20.11	97
	$1 \times 10^{-3}$	1.047	913.5	0.479	0.78	19.93	98

The constant phase element (CPE) could be treated as a parallel combination of a pure capacitor and a resistor being inversely proportional to the angular frequency and its impedance given by:

$$Z_{CPE} = \frac{1}{Q(j\omega)^n} \quad (6)$$

where  $Q$  is the magnitude of the CPE (in  $\Omega^{-1} \times \text{Sn} \times \text{cm}^{-2}$ ),  $j$  is the imaginary unit,  $\omega$  is the angular frequency (in  $\text{rad s}^{-1}$ ;  $\omega = 2\pi f$ , where  $f$  is the AC frequency) and  $n$  is the exponential term of a CPE that can be used as a measure of surface inhomogeneity. To obtain a direct correlation between charge-transfer resistance ( $R_{ct}$ ) and double layer capacitance ( $C_{dl}$ ), the later has been recalculated using the following equation [20]:

$$C_{dl} = \sqrt[n]{Q \times R_{ct}^{1-n}} \quad (7)$$

The percentage inhibition efficiencies  $\eta_{R_{ct}}$  in terms of  $R_{ct}$  are calculated through the following equation:

$$\eta_{R_{ct}} (\%) = \left[ \frac{R_{ct(\text{inh})} - R_{ct}}{R_{ct(\text{inh})}} \right] \times 100 \quad (8)$$

where  $R_{ct(\text{inh})}$  and  $R_{ct}$  are the charge transfer resistance values in with and without inhibitor, respectively. The value of double layer capacitance ( $C_{dl}$ ) and the inhibitory efficiency are also listed in Table 4.

It is apparent from the parameters of Table 4 that the impedance of the inhibited system is amplified with increasing inhibitor concentrations and the  $R_{ct}$  values in the presence of inhibitors are larger than the  $R_{ct}$  for the blank. The increase in  $R_{ct}$  values is attributed to the formation of an insulating protective film of the inhibitors at the metal/solution interface. The CPE value decreases on increasing the concentration of all the three inhibitors, indicating the adsorption of the inhibitor molecules on surface of carbon steel. The values of  $R_{ct}$  increase with the concentration, whilst  $C_{dl}$  values generally decrease. The decrease of  $C_{dl}$  is associated to the increase in thickness of electrical double layer as a result of adsorption of the inhibitor on carbon steel [21-22]. Also it is the manifestation of removal of water molecules and other pre-adsorbed ions (here, chloride) from metal surface by the inhibitor molecules [20]. It is clear that there is a causal relationship between adsorption and inhibition. In addition, it is evident that the inhibitory efficiency increases with increasing inhibitor concentrations. From the table, adsorption capacity, and hence the inhibitive performance are observed to be varied in the series: MSBP > MSVB > EMSB. Furthermore, Table 4 shows that the corrosion inhibition efficiency obtained from EIS measurements is consistent with that obtained from PDP and from weight loss.

### **Temperature effect**

The temperature effect, for 30 mn, on the corrosion behavior of carbon steel in acid solution (HCl 1 M) in absence and of the tested inhibitors at the concentration of  $10^{-3}\text{M}$  is studied in the temperature range of 303-333 K using PDP measurements. The potentiodynamic polarization curves are represented in Figs 5 and 6. Table 5 regroups the obtained corresponding results. From the

experimental data (Table 5) we note that the corrosion current density increases both in the uninhibited and inhibited acid solution, with the rise of temperature. We also notice that the corrosion rate of carbon steel in the absence of inhibitors increased steeply from 303 to 333 K, whereas the corrosion rate increases slowly in the presence of the inhibitors. It is also clear from Table 5 that  $\eta_{\text{PDP}}\%$  decreased with increasing temperature from 303 to 333 K. These results can be described on the basis that the increase in temperature leads to a shift of the equilibrium position of the adsorption/desorption phenomenon towards desorption of the inhibitors molecules at the surface of carbon steel [23].

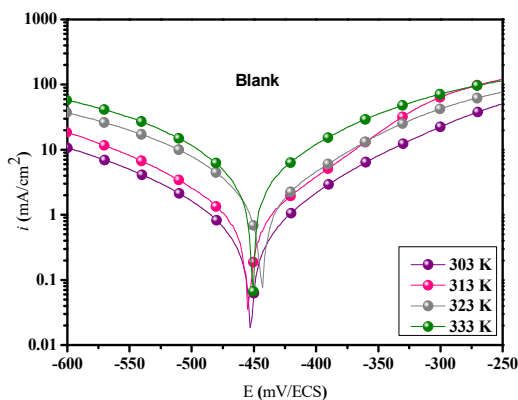


**Figure 5.** Potentiodynamic polarization curves for carbon steel in 1.0 M HCl in the absence of benzimidazole derivatives at different temperatures.

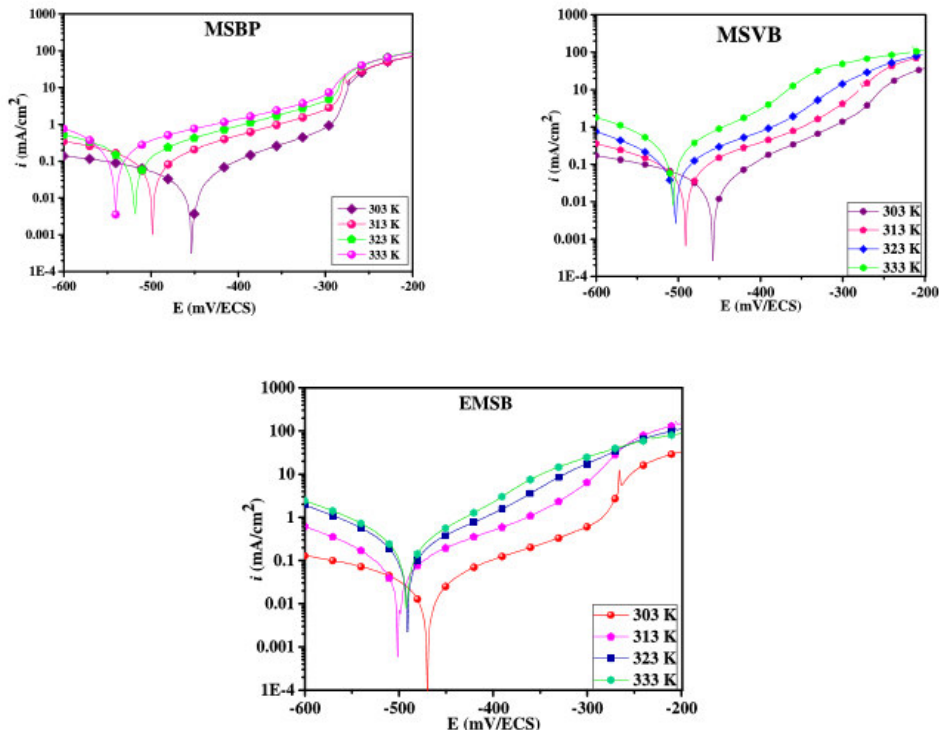


**Figure 6.** Potentiodynamic polarization curves for carbon steel in 1.0 M HCl in the presence of  $10^{-3}$  M of benzimidazole derivatives at different temperatures.

**Table 5.** Corrosion parameters obtained from PDP measurements of carbon steel in 1 M HCl solution in the presence and absence of  $10^{-3}$  M of the inhibitors at different temperatures.

Medium	T (K)	$E_{corr}$ (mV/ECS)	$i_{corr}$ ( $\mu\text{A cm}^{-2}$ )	$\eta_{PDP}$ (%)	$\theta$
Blank	303	-452	507	-	-
	313	-454	860	-	-
	323	-443	1840	-	-
	333	-450	2800	-	-
EMSB	303	-472	41	92	0.92
	313	-503	91	89	0.89
	323	-493	251	86	0.86
	333	-494	616	78	0.78
MSVB	303	-457	26	95	0.95
	313	-490	65	92	0.92
	323	-503	175	90	0.90
	333	-505	361	87	0.87
MSBP	303	-453	16	97	0.97
	313	-497	57	93	0.93
	323	-518	150	92	0.92
	333	-541	283	90	0.90

Additionally, effect of temperature on the nature of carbon steel dissolution in 1 M HCl can be best explained in terms of the Arrhenius equation. The apparent activation energy ( $E_a$ ) for dissolution of carbon steel in 1 M HCl solution without and with various concentrations of the inhibitors was calculated by using the Arrhenius equation (9):

$$i_{corr} = K \exp\left(\frac{-E_a}{RT}\right) \quad (9)$$

where  $E_a$  is the apparent activation energy,  $R$  is the molar gas constant ( $8.314 \text{ J K}^{-1} \text{ mol}^{-1}$ ),  $T$  is the absolute temperature, and  $K$  is the Arrhenius pre-exponential factor. The Arrhenius plots of  $\ln(i_{corr})$  against  $1/T$  for the corrosion of carbon steel in 1 M HCl solution in the absence and presence of various concentrations of EMSB, MSVB and MSBP are shown in Fig. 7. The slopes of the lines were determined and the respective values of  $E_a$  were calculated from the slopes of the plots in Fig. 7. The calculated values of  $E_a$  are listed in Table 6. It is obvious that the presence of  $10^{-3}$  M of the inhibitors in acid media increases the apparent  $E_a$  compared to the blank value. This result indicates a decrease in

the rate of dissolution of carbon steel in the acid due to an increase in energy barrier for the dissolution reaction, which in turn is associated with the adsorption of the inhibitors on the metal surface [24].

The thermodynamic parameters (enthalpy  $\Delta H^\circ$  and entropy  $\Delta S^\circ$  of activation) for corrosion of carbon steel in free 1 M HCl solution, and that containing  $10^{-3}$  M of the inhibitors in HCl 1 M, were calculated from the slopes and intercepts of lines in Fig. 8 using the following equation:

$$i_{corr} = \left(\frac{RT}{Nh}\right) \exp\left(\frac{\Delta S^\circ}{R}\right) \exp\left(\frac{-\Delta H^\circ}{RT}\right) \quad (10)$$

where N is the Avogadro's number and h is the Planck's constant.

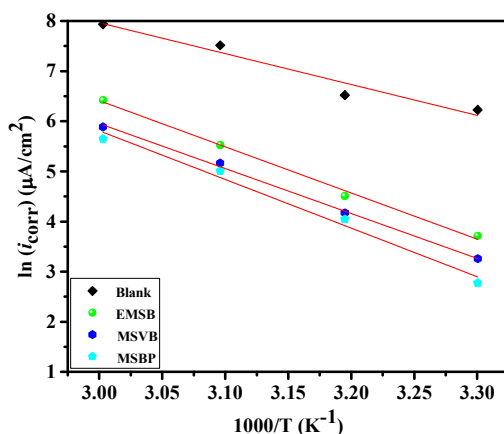


**Figure 7.** Arrhenius plots for C-steel in absence and presence of  $10^{-3}$  M of the inhibitors.

**Table 6.** Activation parameters of the dissolution of C-steel in 1 M HCl with and without  $10^{-3}$  M of benzimidazole derivatives.

Inhibitor	$E_a$ (kJ mol <sup>-1</sup> )	$\Delta H_a$ (kJ mol <sup>-1</sup> )	$\Delta S_a$ (J mol <sup>-1</sup> K <sup>-1</sup> )	$E_a - \Delta H_a$
Blank	49.38	46.77	-38.96	4.48
MSBP	80.70	78.06	36.74	2.64
MSVB	74.56	71.93	19.54	2.63
EMSB	76.60	73.96	29.45	2.64

A plot of  $\ln \frac{i_{corr}}{T}$  against  $\frac{1}{T}$  (Fig. 8) gave straight lines with a slope of  $\frac{-\Delta H^\circ}{R}$  and

an intercept of  $\ln \frac{R}{Nh} + \frac{\Delta S^\circ}{R}$  from which the value of activation thermodynamic

parameters  $\Delta H^\circ$  and  $\Delta S^\circ$  were calculated, being listed in Table 6. The higher value of  $\Delta H$  indicates the creation of an energy barrier for the corrosion reaction in presence of the inhibitor. The positive values of  $\Delta H$  reflect the endothermic nature of the dissolution of the tested alloy in the corrosive media. The negative value of  $\Delta S$  for the three inhibitors indicates that the formation of the activated



complex in the rate determining step represents an association rather than a dissociation step, meaning that a decrease in disorder lines takes place during the course of the transition from reactants to the activated complex [25].

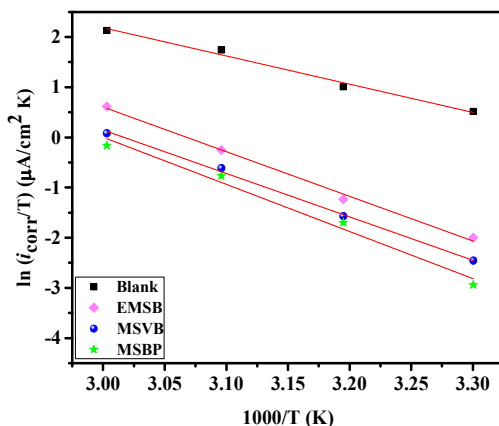
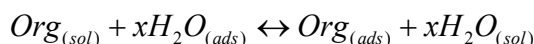


**Figure 8.** Alternative Arrhenius plots for C-steel in absence and presence of  $10^{-3}$  M of the inhibitors.

### Adsorption isotherm

In order to give basic information about the absorptive interaction occurred in the investigated corrosive medium, the adsorption isotherm was studied. The adsorption process is affected by several factors such as the type of the corrosive environment, the chemical structure of an organic inhibitor, the distribution of charge in the molecule, the nature properties of the metal surface, etc. The adsorption of organic molecules from the aqueous solution can be regarded as a quasi substitution process between the organic compound in the aqueous phase [org(sol)] and the water molecules at the electrode surface [ $H_2O_{(ads)}$ ] [26]:



where x is the number of water molecules replaced by one organic inhibitor.  $Org_{(sol)}$  and  $Org_{(ads)}$  represent the organic molecules in the solution and the molecules adsorbed on the steel surface, respectively. In order to find the best adsorption isotherm, which characterizes the adsorption of the investigated benzimidazole inhibitors on the carbon steel surface, different isotherm types were employed to fit the empirical data, such as Langmuir, Frumkin and Temkin adsorption isotherms. In this study, the adsorption mechanism was determined by fitting the  $\theta$  values obtained from potentiodynamic polarization data to obtain the best adsorption isotherm at various concentrations. The experimental data were fitted into various adsorption isotherms but Langmuir isotherm gave the best linear plots. The Langmuir isotherm is described according to equation:

$$\frac{C_{inh}}{\theta} = \frac{1}{K_{ads}} + C_{inh} \quad (11)$$

where  $K_{\text{ads}}$  is the equilibrium constant for the adsorption–desorption process,  $C_{\text{inh}}$  is the molar concentration of the inhibitor in the solution, and  $\theta$  is the degree of surface coverage. The plots of  $C_{\text{inh}}/\theta$  vs.  $C_{\text{inh}}$  yielded straight lines, as shown in Fig. 9. The slope and the correlation coefficient ( $R^2$ ) values for the Langmuir adsorption plots are listed in Table 7. It is seen that Langmuir adsorption plots (Fig. 9) of the inhibitors gave straight lines with excellent correlation coefficient ( $R^2$ ). The results suggest that the adsorptions of benzimidazole inhibitors on steel surface obey the Langmuir adsorption isotherm. From Table 7, it can be seen that  $K_{\text{ads}}$  values for all the three studied inhibitors are relatively high, reflecting the high adsorption ability of these benzimidazole inhibitors on carbon steel surface in the investigated aggressive solution [27]. The interaction can be associated to lone pairs of electrons of N, O and S atoms,  $\pi$ -electrons in each of the studied compounds, and the vacant d-orbitals of iron surface atoms. Using the values of  $K_{\text{ads}}$ , the values of  $\Delta G_{\text{ads}}^\circ$  were evaluated by using the equation:

$$\Delta G_{\text{ads}}^\circ = -RT \ln(K_{\text{ads}} \times 55.5) \quad (12)$$

where  $T$  is the absolute temperature,  $R$  is the gas constant, and 55.5 is the molar concentration of water.

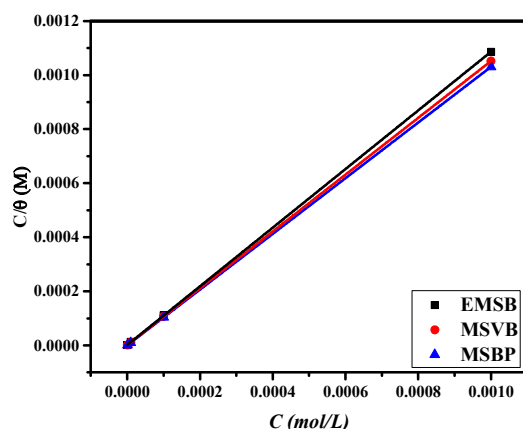


**Figure 9.** Langmuir adsorption plots for carbon steel in 1 M HCl at 303 K containing different concentrations of MSBP, MSVB and EMSB.

It can also be seen from table 7 that  $\Delta G_{\text{ads}}^\circ$  values are negative. This indicates the spontaneity of adsorption and the stability of the adsorbed layer on carbon steel surface [28]. In general, the values of  $\Delta G_{\text{ads}}^\circ$  up to  $-20 \text{ kJ mol}^{-1}$  are associated with the electrostatic interaction between charged inhibitor molecules and charged metal surface (physisorption), and those which are more negative than  $-40 \text{ kJ mol}^{-1}$  involve charge sharing or charge transfer from the inhibitor molecules to the metal surface (chemisorption) [29]. In this study, the calculated  $\Delta G_{\text{ads}}^\circ$  values for EMSB, MSVB and MSBP were found in the range of  $-43.7$  to  $-46.5$ , suggesting that the adsorption process involved a predominance of the chemical adsorption.

**Table 7.** Thermodynamic parameters for the adsorption of MSBP, MSVB and EMSB calculated from Langmuir adsorption isotherm for carbon steel at 303 K.

Inhibitors	$R^2$	$K_{ads}(M^{-1})$	$\Delta G_{ads}(kJ/mol)$
MSBP	1.00	1939600	-46.5
MSVB	1.00	851571	-44.1
EMSB	1.01	633793	-43.7

### Computational studies

#### DFT calculations

In order to afford insights on the structural and electronic properties of the various active constituents of the studied benzimidazole derivatives, DFT calculations were employed, particularly since the molecular structure is one of the major factors influencing the adsorption of the organic molecules on the metal surface, and hence the inhibitor properties, especially in the case of chemisorption, which involves charge sharing or charge transfer from the inhibitor molecules to the metal to form coordinate type of bonds. So the influence of the chemical structure is limited to the molecular area in the adsorbed state, because it determines the area of the metal, shielded by the inhibitor. Through geometrical optimization and investigating frontier molecular orbitals (FMO), highest occupied molecular orbital (HOMO) and lowest unoccupied molecular orbital (LUMO), one can predict the nature, as well as the extent, of adsorption of the inhibitor molecules [30-31]. The adsorption of organic compounds on metallic surface occurs principally through donor-acceptor interaction. It is generally assumed that, electron donating ability of a molecule increases with increasing  $E_{HOMO}$  value, whereas lower value of  $E_{LUMO}$  indicates the molecule to be more susceptible towards accepting electrons [32-33]. Fig. 10 presents the optimized structures, HOMO and LUMO electron density surfaces of the studied molecules. The corresponding calculated quantum chemical parameters such as  $E_{HOMO}$ ,  $E_{LUMO}$ ,  $\Delta E$ , and  $\Delta N$ , are represented in Table 8. The ionization potential (IP), and electron affinity (EA), were deduced from  $E_{HOMO}$  and  $E_{LUMO}$  using Eqs. (13) and (14):

$$IP = -E_{HOMO} \quad (13)$$

$$EA = -E_{LUMO} \quad (14)$$

Meanwhile, electronegativity ( $\chi$ ) and chemical hardness ( $\eta$ ) were evaluated, based on the finite difference approximation, using the following relations [34-35]:

$$\chi = \frac{IP + EA}{2} \quad (15)$$

$$\eta = \frac{IP - EA}{2} \quad (16)$$

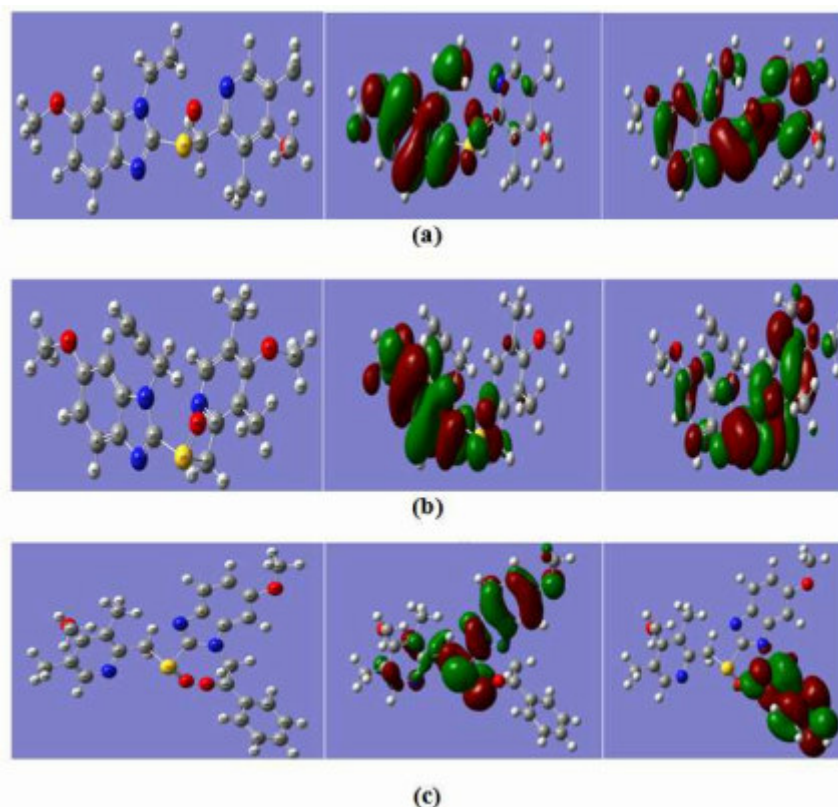


**Figure 10.** The optimized structure (left), HOMO (center), and LUMO (right), distribution for molecules (a) EMSB, (b) MSVB and (c) MSBP. [Atom legend: white = H; Cyan = C; blue = N; red = O].

Kokalj recently reported [36] that the work function ( $\phi$ ) of a metal surface is an appropriate measure of its electronegativity and should be used together with its vanishing absolute hardness to estimate the fraction of electrons transferred ( $\Delta N$ ), using the equation:

$$\Delta N = \frac{\phi - \chi_{inh}}{2(\eta_{Fe} + \eta_{inh})} \quad (17)$$

where ( $\phi$ ) and  $\chi_{inh}$  denote the work function and absolute electronegativity of iron and inhibitor molecule, respectively,  $\eta_{Fe}$  and  $\eta_{inh}$  denote the absolute hardness of iron and the inhibitor molecule, respectively. Theoretical  $\chi_{Fe}$  and  $\eta_{Fe}$  values for carbon steel of 7 and 0, respectively, were considered in order to calculate the  $\Delta N$  values. In this simulation, the obtained DFT derived ( $\phi$ ) value for Fe (110) surface is 4.82 eV, because Fe (110) has higher stabilization energy and packed surface [36-37]. The molecule with the highest  $E_{HOMO}$  values indicates that this molecule has a high tendency to donate electrons to appropriate acceptor molecules with low energy empty molecular orbitals. The lower value of  $E_{LUMO}$  for a molecule suggests that the molecule can readily accept electrons from the donor molecules [38]. As a result, the molecule with lower absolute value of the

energy band gap ( $\Delta E = E_{\text{LUMO}} - E_{\text{HOMO}}$ ) exhibits higher inhibition efficiencies because of the possibility of both ways of electron transfer, i.e., inhibitor to metal and vice versa [39-40].

**Table 8.** Calculated quantum chemical properties for the inhibitors benzimidazole derivatives obtained from DFT method.

Inhibitors	$E_{\text{HOMO}}$ (eV)	$E_{\text{LUMO}}$ (eV)	$\Delta E_{\text{gap}}$ (eV)	$\Delta N$
EMSB	-5.687	-1.261	4.425	0.304
MSVB	-5.528	-1.284	4.244	0.314
MSBP	-5.501	-1.706	3.795	0.338

Upon inspection of the results, we noticed that the reactivity of the selected organic constituents would likely depend on their molecular structure. For all the three benzimidazole derivatives, the HOMO and LUMO orbitals are  $\pi$ -type orbitals and the electron densities are essentially delocalized over the benzimidazole ring, the adjacent pyridin group, and phenacyl group in the case of molecule MSBP.  $E_{\text{HOMO}}$  is seen to increase following the order, EMSB < MSVB < MSBP, demonstrating enhanced ability of the inhibitor molecules to interact with metal surface through electron donation (HOMO of the inhibitors to vacant d-orbital of Fe).  $E_{\text{LUMO}}$  follows the reverse order. This manifests that electron accepting ability (from filled 4 s orbital of Fe to LUMO of the inhibitors) increases following the trend EMSB < MSVB < MSBP. In addition, the energy band gap ( $\Delta E$ ) reflects the reactivity of the inhibitor molecule toward the adsorption on the metal surface [41]. If  $\Delta E$  increases, the reactivity of the molecule brings down, which may retard adsorption and decrease the inhibition efficiency. By the inspection of Table 8, we can find that MSBP has lower  $\Delta E$  value, which suggests that MSBP has more potency to get adsorbed on the carbon steel surface, resulting in greater inhibition tendency than MSVB and EMSB. The reason for this is likely related to the presence of more important reactive centers in MSBP inhibitor (presence of additional hetero atoms like O, heterocyclic ring, and double bonds in conjugated system). These outcomes are in well accordance with the result obtained from experimental studies.

Furthermore,  $\Delta N$  value is another important index that measures the ability of a chemical compound to transfer electrons. Electron transfer will occur from inhibitor molecule to metal surface if  $\Delta N > 0$  and vice versa if  $\Delta N < 0$  [42,-43]. According to Elnga et al., [44] inhibition efficiency increases with increasing electron-donating ability of the molecule at the metal surface if  $\Delta N < 3.6$ . In Table 8, all the values of  $\Delta N$  are positive and less than 3.6, indicating that the molecules donate their electrons to the Fe surface by the formation of a coordinate bond. As expected, MSBP had the highest positive  $\Delta N$  values compared to other inhibitors, which agrees well with the trend of  $\Delta E$ . In this study, the inhibition efficiency of MSBP is due to the centres of adsorption on the inhibitor molecules ( $=\text{N}-$ ,  $-\text{O}-$ ,  $=\text{O}$  and  $-\text{S}=\text{O}$ ) and the higher electron

density caused by the electron releasing methoxy groups ( $\text{OCH}_3$ ). In view of this, it is reasonable to propose that the high and stable inhibiting efficacy obtained experimentally is related to the multi-component adsorption process and/or the synergistic effect of the multi-constituents in the benzimidazole derivatives adsorbing on the steel surface. The graphical surfaces of the electron charge density with Mulliken charges, according to the numeration of corresponding atoms of the optimized structures of the inhibitors, are shown in Fig. 11. The general interpretation given by several authors is that the higher is the magnitude and the number of negatively charged heteroatom present in an inhibitor molecule, the higher the ability to be adsorbed on the metal surface via donor–acceptor mechanism [45]. It is clear from Fig. 11 that all the three inhibitors have considerable excess of negative charge around the nitrogen atoms in the benzimidazole ring, benzene ring, and oxygen of the methoxy group, and also on some carbon atoms. This suggests that these centers are the coordinating sites through which the inhibitors will adsorb on a positively charged metal surface.

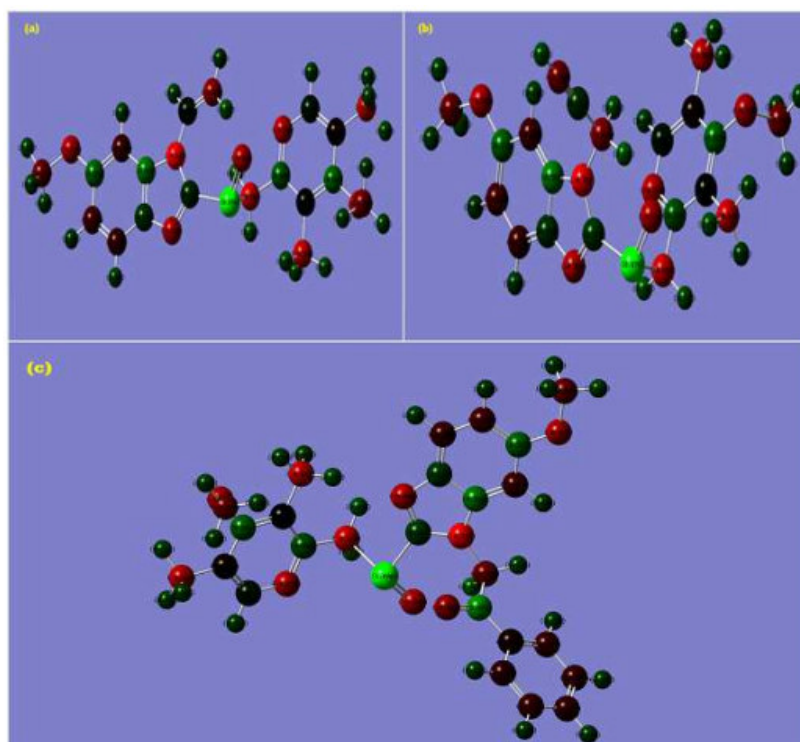


**Figure 11.** The Mulliken charge density of (a) EMSB, (b) MSVB and (c) MSBP.

#### *Molecular Dynamics (MD) simulation*

MD simulations are a modern tool to research the adsorption behavior of the inhibitor molecules on the Fe(110) surface, and therefore predict the adsorption ability of the inhibitors when adsorption process has reached equilibration. The system reaches equilibrium only if both of the energy and temperature reach balance. In our present study, the MD simulations calculation was used to find interaction energy for the investigated systems. The strong adsorption between the inhibitors and the iron surface are reflected from their high negative



interaction energy values. The best adsorption configurations of benzimidazole derivative on Fe(110) surface obtained through the MD simulations are depicted in Fig. 12.

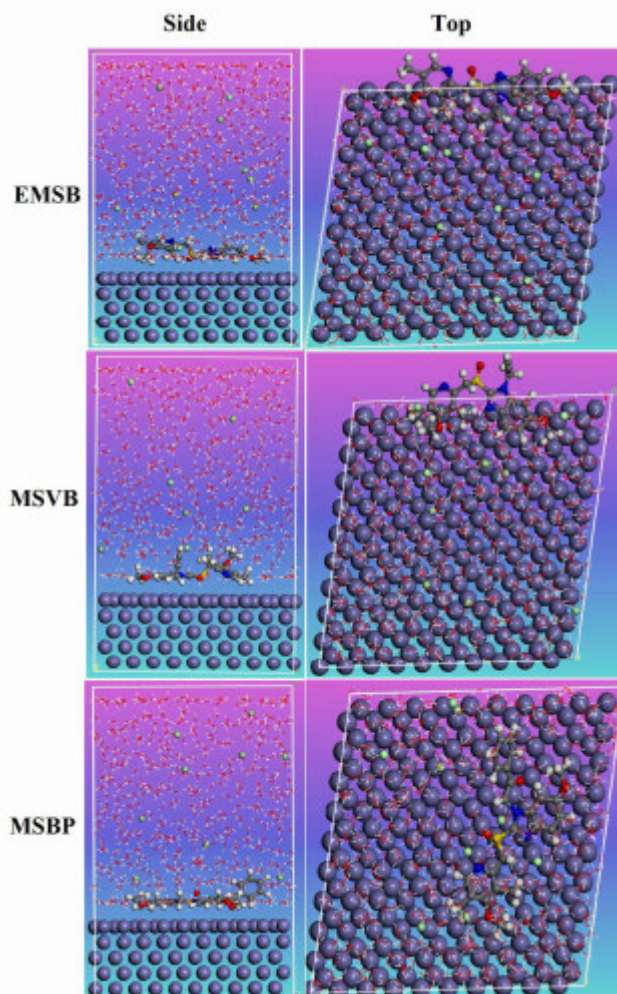


**Figure 12.** Side and top views of the final adsorption of the benzimidazole derivatives on the Fe(110) surface in solution.

The corresponding values of the interaction energies between the inhibitor and Fe(110) surface are listed in Table 9. As can be seen from Fig. 12, at equilibrated state, the benzimidazole derivatives adsorb on the Fe(1 1 0) surface with a nearby flat orientation between the rigid structure and the metal surface. Due to the presence of unoccupied 3d-orbitals of the metal, it will prefer to accept electrons from the adsorbed inhibitor molecule. The heteroatoms and  $\pi$ -electrons present in benzimidazole derivatives, and substituted groups ( $-OCH_3$ ), will certainly provide sufficient electrons to the vacant metal 3d-orbitals for the formation of stable coordination bond. On the other hand, antibonding orbital of  $\pi$ -electrons in the benzimidazole and pyridine ring can also accept the electrons from 4s or 3d-orbital of iron to form feedback bonds. More interesting, the inhibitor film adsorption energies presented in Table 9, revealed very high negative values and decreased in the order: MSBP>MSVB>EMSb. Also, all the values of interaction energies are negative, which denotes that the adsorption could occur spontaneously [46-47]. Consequently, the highest value of interaction energy for

MSBP (Table 9) suggests that it is the best stable adsorption system among the studied benzimidazoles derivatives, and thus explains its high corrosion inhibition efficiency. All these results are in good agreement with the results obtained from experimental work, as well as from quantum chemical calculations.

**Table 9.** Energy parameters obtained from MD simulations for adsorption of the inhibitors on Fe(110) surface.

System	$E_{\text{Interaction}}$ (kcal/mol)	$E_{\text{Binding}}$ (kcal/mol)
Fe + EMSB + 491 H <sub>2</sub> O + 9 Cl <sup>-</sup> + 9 H <sub>3</sub> O <sup>+</sup>	-723.081	723.081
Fe + MSVB + 491 H <sub>2</sub> O + 9 Cl <sup>-</sup> + 9 H <sub>3</sub> O <sup>+</sup>	-536.104	536.104
Fe + MSBP + 491 H <sub>2</sub> O + 9 Cl <sup>-</sup> + 9 H <sub>3</sub> O <sup>+</sup>	-413.003	413.003

### SEM study

Using Scanning Electron Micrographs (SEM), the surfaces of mild steel are recorded in order to evaluate the changes occurred during the corrosion process in absence and presence of  $5 \times 10^{-3}$  M of MSBP, supporting our conclusion that this inhibitor is an efficient corrosion inhibitor in the studied conditions. Fig. 13 depicts the surface photo micrographs of the steel exposed to 1 M HCl in the absence and presence of MSBP. Considering the result of the SEM study, it can be clearly observed that the surface of mild steel in the uninhibited solution (Fig. 13a) is seriously damaged and heterogeneous because of severe corrosion of mild steel by the aggressive acid, indicating a direct acid attack on the metal and high corrosion rate without the presence of any inhibitor. However, the surface heterogeneity is considerably decreased in the presence of the inhibitor MSBP (Fig. 13b). Furthermore, the relatively smooth surface observed in the presence of the inhibitor would have been caused by the deposition of the inhibitor on the mild steel surface, and consequently the formation of the protective film of the inhibitor which shields the surface against direct acid attack.

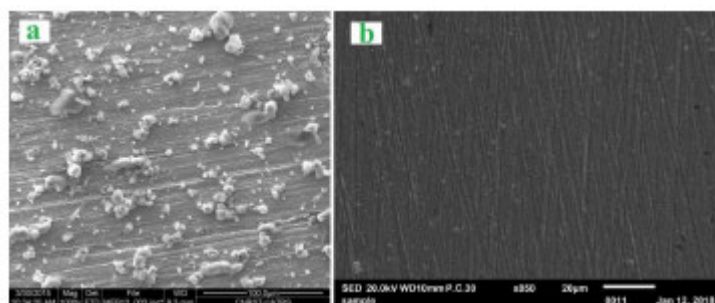


**Figure 13.** SEM images of mild steel surface after immersion for 6 h in (a) 1.0 M HCl without inhibitor, and (b) 1.0 M HCl +  $5 \times 10^{-3}$  M of MSBP.



## Conclusion

This work exemplifies the effect of the nature of substituent groups on corrosion inhibition propensity of benzimidazole derivatives towards carbon steel in 1 M HCl. Main conclusions are summarized here:

1. The inhibitors benzimidazole derivatives (EMSB/MSVB/MSBP) show good inhibition efficiency for the protection of carbon steel in 1 M HCl solution and the inhibition efficiency increases on increasing the concentration of the inhibitors and decreases with increase in temperature. The order of the inhibition efficiency is: MSBP > MSVB > EMSB.
2. Potentiodynamic polarization studies reveal the benzimidazole derivatives to have the properties corresponding to mixed type inhibitors.
3. Impedance results revealed that the corrosion inhibition action was due to the adsorption of the various organic constituents of benzimidazole derivatives on the carbon steel surface and the adsorption process followed Langmuir adsorption isotherm.
4. The thermodynamic parameters indicated that the adsorption process of the tested molecules on the steel was endothermic and the calculated values of  $\Delta G_{\text{ads}}^{\circ}$  reveal that the adsorption mechanism of EMSB, MSVB and MSBP on the carbon steel surface is mainly chemisorption.
5. The inhibitor efficiencies of these compounds seem to be determined by the conjugation of electronic factors and molecular geometry. The analysis of the HOMO, LUMO, and partial atomic charges suggests the centers that would be preferred for nucleophilic or electrophilic attack.
6. Molecular dynamic simulations performed on the individual active constituents revealed strong to reasonable adsorption strengths for most of the active species and the large negative value of adsorption energy in Monte Carlo simulations indicates the strong interaction between the metal and the investigated inhibitors.
7. Planar molecular configuration, lowest energy gap between the frontier molecular orbitals, presence of pyridine and benzene ring connected with benzimidazole and other favorable molecular factors have made MSBP as the most efficient corrosion inhibitor among all the three inhibitors of the present work.

## References

1. Popova A, Christov M, Raicheva S, et al. Adsorption and inhibitive properties of benzimidazole derivatives in acid mild steel corrosion. *Corros Sci.* 2004;46:1333–1350.
2. Popova A, Christov M, Deligeorgiev T. Influence of the molecular structure on the inhibitor properties of benzimidazole derivatives on mild steel corrosion in 1 M hydrochloric acid. *Corrosion.* 2003;59:756–764.
3. Wang X, Yang H, Wang F. An investigation of benzimidazole derivative as corrosion inhibitor for mild steel in different concentrations of HCl solutions. *Corros Sci.* 2011;53:113–121.

4. Baviskar BA, Baviskar B, Shiradkar MR, et al. Synthesis and Antimicrobial Activity of Some Novel Benzimidazolyl Chalcones. *J Chem.* 2009;6:196–200.
5. Khaled KF. The inhibition of benzimidazole derivatives on corrosion of iron in 1 M HCl solutions. *Electrochim Acta.* 2003;48:2493–2503.
6. Abboud Y, Abourriche A, Saffaj T, et al. The inhibition of mild steel corrosion in acidic medium by 2, 2'-bis (benzimidazole). *Appl Surf Sci.* 2006;252:8178–8184.
7. Aljourani J, Raeissi K, Golozar MA. Benzimidazole and its derivatives as corrosion inhibitors for mild steel in 1M HCl solution. *Corros Sci.* 2009;51:1836–1843.
8. Popova A, Christov M. Evaluation of impedance measurements on mild steel corrosion in acid media in the presence of heterocyclic compounds. *Corros Sci.* 2006;48:3208–3221.
9. Popova A, Sokolova E, Raicheva S, et al. AC and DC study of the temperature effect on mild steel corrosion in acid media in the presence of benzimidazole derivatives. *Corros Sci.* 2003;45:33–58.
10. Popova A, Christov M, Zwetanova A. Effect of the molecular structure on the inhibitor properties of azoles on mild steel corrosion in 1M hydrochloric acid. *Corros Sci.* 2007;49:2131–2143.
11. Aljourani J, Golozar MA, Raeissi K. The inhibition of carbon steel corrosion in hydrochloric and sulfuric acid media using some benzimidazole derivatives. *Mater Chem Phys.* 2010;121:320–325.
12. Zhang Z, Tian N, Huang X, et al. Synergistic inhibition of carbon steel corrosion in 0.5 M HCl solution by indigo carmine and some cationic organic compounds: experimental and theoretical studies. *RSC Adv.* 2016;6:22250–22268.
13. Ezeoke AU, Adeyemi OG, Akerele OA, et al. Computational and experimental studies of 4-aminoantipyrine as corrosion inhibitor for mild steel in sulphuric acid solution. *Int J Electrochem Sci.* 2012;7:534–553.
14. ang H-L, Fan H-B, Zheng J-S. Corrosion inhibition of mild steel in hydrochloric acid solution by a mercapto-triazole compound. *Materials Chemistry and Physics.* 2003;77(3):655–661.
15. Zhang QB, Hua YX. Corrosion inhibition of mild steel by alkylimidazolium ionic liquids in hydrochloric acid. *Electrochim Acta.* 2009;54:1881-1887.
16. Bentiss F, Lebrini M, Vezin H, et al. Experimental and theoretical study of 3-pyridyl-substituted 1, 2, 4-thiadiazole and 1, 3, 4-thiadiazole as corrosion inhibitors of mild steel in acidic media. *Mater Chem Phys.* 2004;87-18-23.
17. Ferreira ES, Giacomelli C, Giacomelli FC, et al. Evaluation of the inhibitor effect of L-ascorbic acid on the corrosion of mild steel. *Mater Chem Phys.* 2004;83:129-134.
18. de Souza FS, Spinelli A. Caffeic acid as a green corrosion inhibitor for mild steel. *Corros Sci.* 2009;51:642-649.
19. Ashassi-Sorkhabi H, Shaabani B, Seifzadeh D. Corrosion inhibition of mild steel by some Schiff base compounds in hydrochloric acid. *Appl Surf Sci.* 2005;239:154-164.

20. Lebrini M, Robert F, Roos C. Inhibition effect of alkaloids extract from *Annona squamosa* plant on the corrosion of C38 steel in normal hydrochloric acid medium. *Int J Electrochemi Sci.* 2010;5:1698-1712.
21. Tang Y, Zhang F, Hu S, et al. Novel benzimidazole derivatives as corrosion inhibitors of mild steel in the acidic media. Part I: gravimetric, electrochemical, SEM and XPS studies. *Corros Sci.* 2013;4:271-282.
22. Daoud D, Douadi T, Hamani H, et al. Corrosion inhibition of mild steel by two new S-heterocyclic compounds in 1 M HCl: experimental and computational study. *Corros Sci.* 2015;94:21-37.
23. Fragoza-Mar L, Olivares-Xometl O, Domínguez-Aguilar MA, et al. Corrosion inhibitor activity of 1, 3-diketone malonates for mild steel in aqueous hydrochloric acid solution. *Corros Sci.* 2012;61:171-184.
24. Oguzie EE. Evaluation of the inhibitive effect of some plant extracts on the acid corrosion of mild steel. *Corros Sci.* 2008;50:2993–2998.
25. Ramesh SV, Adhikari AV. Corrosion inhibition of mild steel in acid media by quinolinyl thiopropano hydrazone. *Indian J Chem Technol.* 2009;16:162-174.
26. Wang X, Yang H, Wang F. A cationic gemini-surfactant as effective inhibitor for mild steel in HCl solutions. *Corros Sci.* 2010;52: 1268-1276.
27. Migahed MA. Electrochemical investigation of the corrosion behaviour of mild steel in 2M HCl solution in presence of 1-dodecyl-4-methoxy pyridinium bromide. *Mater Chem Phys.* 2005;93:48-53.
28. Fouda AS, Heakal FE, Radwan MS. Role of some thiadiazole derivatives as inhibitors for the corrosion of C-steel in 1 M H<sub>2</sub>SO<sub>4</sub>. *J Appl Electrochem.* 2009;39:391-402.
29. Behpour M, Ghoreishi SM, Soltani N, et al. Electrochemical and theoretical investigation on the corrosion inhibition of mild steel by thiosalicylaldehyde derivatives in hydrochloric acid solution. *Corros Sci.* 2008;50: 2172-2181.
30. Ehsani A, Mahjani MG, Moshrefi R, et al. Electrochemical and DFT study on the inhibition of 316L stainless steel corrosion in acidic medium by 1-(4-nitrophenyl)-5-amino-1 H-tetrazole. *RSC Adv.* 2014;4:20031-20037.
31. Dutta A, Saha SK, Banerjee P, et al. Evaluating corrosion inhibition property of some Schiff bases for mild steel in 1 M HCl: competitive effect of the heteroatom and stereochemical conformation of the molecule. *RSC Adv.* 2016;6:74833-74844.
32. Fu J, Zang H, Wang Y, et al. Experimental and theoretical study on the inhibition performances of quinoxaline and its derivatives for the corrosion of mild steel in hydrochloric acid. *Ind Eng Chem Res.* 2012;51:6377-6386.
33. Obot I, Gasem Z, Umoren S. Molecular level understanding of the mechanism of aloes leaves extract inhibition of low carbon steel corrosion: a DFT approach. *Int J Electrochem Sci.* 2014;9:510-522.
34. Pearson RG. Absolute electronegativity and hardness: application to inorganic chemistry. *Inorg Chem.* 1988;27:734-740.
35. Sastri V, Perumareddi J. Molecular orbital theoretical studies of some organic corrosion inhibitors. *Corrosion.* 1997;53:617-622.

36. Kokalj A. On the HSAB based estimate of charge transfer between adsorbates and metal surfaces. *Chem Phys.* 2012;393:1-12.
37. Saha SK, Murmu M, Murmu NC, et al. Evaluating electronic structure of quinazolinone and pyrimidinone molecules for its corrosion inhibition effectiveness on target specific mild steel in the acidic medium: A combined DFT and MD simulation study. *J Mol Liq.* 2016;224:629-638.
38. Xia S, Qiu M, Yu L, et al. Molecular dynamics and density functional theory study on relationship between structure of imidazoline derivatives and inhibition performance. *Corros Sci.* 2008;50:2021-2029.
39. Obot I, Gasem Z. Theoretical evaluation of corrosion inhibition performance of some pyrazine derivatives. *Corros Sci.* 2014;83:359-366.
40. Dutta A, Saha SK, Banerjee P, et al. Evaluating corrosion inhibition property of some Schiff bases for mild steel in 1 M HCl: competitive effect of the heteroatom and stereochemical conformation of the molecule. *RSC Adv.* 2016;6:74833-74844.
41. Gao G, Liang C. Electrochemical and DFT studies of  $\beta$ -amino-alcohols as corrosion inhibitors for brass. *Electrochim Acta.* 2007;52:4554-4559.
42. Kokalj A. Is the analysis of molecular electronic structure of corrosion inhibitors sufficient to predict the trend of their inhibition performance. *Electrochim Acta.* 2010;56:745-755.
43. Kovačević N, Kokalj A. Analysis of molecular electronic structure of imidazole- and benzimidazole-based inhibitors: A simple recipe for qualitative estimation of chemical hardness. *Corros Sci.* 2011;53:909-921.
44. Awad MK, Mustafa MR, Elnga MMA. Computational simulation of the molecular structure of some triazoles as inhibitors for the corrosion of metal surface. *J Mol Struct: Theochem.* 2010;959:66-74.
45. Yadav DK, Maiti B, Quraishi M. Electrochemical and quantum chemical studies of 3, 4-dihydropyrimidin-2 (1H)-ones as corrosion inhibitors for mild steel in hydrochloric acid solution. *Corros Sci.* 2010;52:3586-3598.
46. Obot I, Gasem Z. Theoretical evaluation of corrosion inhibition performance of some pyrazine derivatives. *Corros Sci.* 2014;83:359-366.
47. Obot I, Umoren S, Gasem Z, et al. Theoretical prediction and electrochemical evaluation of vinylimidazole and allylimidazole as corrosion inhibitors for mild steel in 1M HCl. *J Ind Eng Chem.* 2015;21:1328-1339.